J. Fluid Mech. (2014), *vol.* 758, *pp.* 702–727.

doi:10.1017/jfm.2014.521

Streamwise vortex-induced vibrations of cylinders with one and two degrees of freedom

N. Cagney[1] **and S. Balabani**[2,†]

[1]Department of Earth Sciences, University College London, Gower Street, London WC1E 6BT, UK

[2]Department of Mechanical Engineering, University College London, Torrington Place, London WC1E 7JE, UK

(Received 2 May 2014; revised 16 July 2014; accepted 4 September 2014; first published online 13 October 2014)

Measurements are presented of the structural response and wake of a two-degree-of-freedom (2-DOF) pivoted cylinder undergoing streamwise vortex-induced vibrations (VIV), which were carried out using particle-image velocimetry (PIV). The results are compared with those of previous studies performed in the same experimental facility examining a cylinder free to move only in the streamwise direction (1-DOF). The aim of this study is to examine to what extent the results of previous work on streamwise-only VIV can be extrapolated to the more practical, multi-DOF case. The response regimes measured for the 1- and 2-DOF cases are similar, containing two response branches separated by a low-amplitude region. The first branch is characterised by negligible transverse motion and the appearance of both alternate and symmetric vortex shedding. The two wake modes compete in an unsteady manner; however, the competition does not appear to have a significant effect on either the streamwise or transverse motion. Comparison of the phase-averaged vorticity fields acquired in the second response branch also indicates that the additional DOF does not alter the vortex-shedding process. However, the additional DOF affects the cylinder-wake system in other ways; for the 1-DOF case the second branch can appear in three different forms (each associated with a different wake mode), while for the 2-DOF case the second branch only exists in one form, and does not exhibit hysteresis. The cylinder follows a figure-of-eight trajectory throughout the lock-in range. The phase angle between the streamwise and transverse motion decreases linearly with reduced velocity. This work highlights the similarities and differences between the fluid–structure interaction and wake dynamics associated with 1- and 2-DOF cylinders throughout the streamwise response regime, which has not received attention to date.

Key words: flow–structure interactions, vortex dynamics, wakes

1. Introduction

Vortex-induced vibrations (VIV) is a classical fluid–structure interaction problem, affecting a wide range of industrial applications such as marine risers, off-shore

† Email address for correspondence: s.balabani@ucl.ac.uk

structures, tall chimneys, bridges and heat exchangers. Over the past few decades it has been the focus of much research and the topic of a number of review papers (Bearman 1984; Sarpkaya 2004; Williamson & Govardhan 2004).

The mechanism controlling VIV was first identified by Feng (1963), who showed that a bluff body in crossflow can experience vibrations when the fluid forces associated with the periodic shedding of vortices from the structure coincides with its natural frequency, f_n. This resonance can lead to large-amplitude vibrations, which can in turn cause the vortex-shedding frequency to become synchronised to the cylinder motion, a condition known as 'lock-in'. The feedback between the structural motion and vortex shedding is highly complex, and can lead to a wide variety of arrangements of vortices in the wake ('wake modes') and response branches (Khalak & Williamson 1999), as well as phenomena such as hysteresis, added mass and multiple stability states (Aguirre 1977; Govardhan & Williamson 2000; Morse & Williamson 2010).

The frequency of vortex shedding, f_{vs}, from a cylinder is proportional to the freestream velocity, U_0, and is typically non-dimensionalised as the Strouhal number, $St = f_{vs}D/U_0$, where D is the cylinder diameter. The Strouhal number is approximately 0.2 for fixed cylinders. The structural response of a cylinder experiencing VIV is controlled by the reduced velocity, $U_r = U_0/f_nD$. As the lift force associated with vortex shedding occurs at the shedding frequency, while the drag force occurs at twice this value, lock-in (i.e. resonance) can be expected to occur in the transverse and streamwise directions at $U_r \approx 1/St$ and $1/2St$, respectively. (Here the streamwise direction is defined as the flow or drag direction, and the transverse direction is the lift direction.) The apparent mass of the cylinder is the sum of its true or 'dry' mass and the 'added mass', which affects all bodies accelerating in a fluid and is a function of the cylinder acceleration, the vortex-shedding and the associated fluid forces (Sarpkaya 2004). This can cause the cylinder vibration frequency, f_x, to vary from f_n, especially for the case of light cylinders. To account for this, the reduced velocity can be expressed as $U_r/f^* = U_0/f_xD$ (where $f^* = f_x/f_n$), henceforth referred to simply as the reduced velocity.

The vast majority of experimental, numerical and theoretical work investigating VIV has focused on cylinders which are free to move only in one direction, as this is thought to simplify the problem. In most cases, researchers have examined transverse VIV, i.e. VIV of a cylinder free to move only normal to the flow, as the amplitude response in this direction, A_y, tends to be an order of magnitude larger than that occurring in the streamwise direction, A_x (Griffin & Ramberg 1976).

Early work by Sarpkaya (1995) and Jauvtis & Williamson (2003) indicated that the response regime of a 2-DOF cylinder was similar to that measured for transverse-only VIV, i.e. the freedom of the cylinder to move in the streamwise direction did not have a significant effect on the wake dynamics or fluid–structure interaction. However, later work by Williamson & Jauvtis (2004) showed that when the cylinder mass ratio (m^* = (cylinder mass)/(displaced fluid mass)) was lower than approximately 5, the additional DOF caused the appearance of a new response branch, the 'super-upper' branch, which was associated with a significant increase in the amplitude response in both directions and the formation of a new wake mode. Related work examining pivoted (Flemming & Williamson 2005) and two-dimensional cylinders (i.e. cylinders which had a uniform amplitude along their span) (Sanchis, Saelevik & Grue 2008), also found that when $m^* \lesssim 5$, the freedom to move in the streamwise direction caused a significant increase in the response amplitude. A later study by Leong & Wei (2008) showed that cylinders with very low mass ratios (below the critical value of $m^* \approx 0.52$

(Govardhan & Williamson 2002)) can exhibit very large-amplitude vibrations in both directions (over four diameters peak-to-peak) compared with the 1-DOF case.

It is clear that the freedom to move in both the streamwise and transverse directions has a significant effect on VIV, and further work is needed to extend the knowledge of VIV of single-DOF structures to the more practical multi-DOF case. While some work has been performed which analyses the effect of the additional DOF on the transverse response regimes (i.e. where $U_r/f^* \sim 1/St$) (Williamson & Jauvtis 2004; Sanchis *et al.* 2008; Dahl *et al.* 2010), very little is known about how the streamwise response regime is affected. The following subsections summarise the wake dynamics and structural response of 1- and 2-DOF cylinders in the streamwise response regime, and outline the aims of this paper.

1.1. *Streamwise response regime*

In the last decade there has been renewed interest in the case of streamwise-only VIV, following the failure of the 'Monju' reactor due to streamwise vibrations. The streamwise response regime was characterised by Aguirre (1977) (summarised by Naudascher (1987)), while later work by Okajima and colleagues (Nakamura, Okajima & Kosugi 2001; Okajima, Kosugi & Nakamura 2001, 2002; Okajima *et al.* 2003) investigated the sensitivity of the amplitude response to structural parameters such as the mass and damping. Recent work by the current authors presented time-resolved particle-image velocimetry (PIV) measurements of the wake and structural motion of a cylinder undergoing streamwise VIV (Cagney & Balabani 2013*a*,*b*,*c*).

The response regime is characterised by two branches, separated by a region of low-amplitude vibrations at $U_r/f^* \approx 1/2St$ (Aguirre 1977; Okajima *et al.* 2003; Cagney & Balabani 2013*c*). The maximum amplitude in both branches is of the order $A_x/D \sim 0.1$. The first branch occurs in the range $U_r/f^* \approx 1.5$–2.5, and is typically associated with 'wake breathing' or symmetric vortex shedding (Naudascher 1987; Jauvtis & Williamson 2003), in which the streamwise motion of the cylinder causes the shear layers to roll up simultaneously at the same frequency as the cylinder motion, $f_{vs} = f_x$. This vortex pattern is referred to as the S-I mode (following the notation of Ongoren & Rockwell (1988)) and is depicted in figure 1. However, Aguirre (1977) and Cagney & Balabani (2013*c*) showed that for much of this branch, the vortices are actually shed in an alternate pattern, similar to the von Kármán street observed behind stationary cylinders. This mode (the A-II mode, shown in figure 1) also dominates outside the first and second response branches, when the cylinder response is negligible (Cagney & Balabani 2013*c*).

Cagney & Balabani (2013*a*) showed that at certain reduced velocities within the first branch, the wake switches between the S-I and A-II modes in an apparently random manner. Furthermore, the symmetric arrangement of vortices for the S-I mode was found to be unstable, and tended to rearrange downstream into an alternate pattern. This has also been observed in the wake of cylinders undergoing forced streamwise oscillations (Ongoren & Rockwell 1988) and fixed cylinders in pulsating flow (Konstantinidis & Balabani 2007; Perdikaris, Kaiktsis & Triantafyllou 2009). This bimodal behaviour causes the velocity fluctuations in the near wake to occur at f_x, while in the far wake the fluctuations occur at the Strouhal frequency (Cagney & Balabani 2013*a*).

The second branch occurs in the range $U_r/f^* \approx 2.5$–3.5, and is characterised by alternate vortex shedding. The response regime is hysteretic in this region; the extent of the second branch and the lock-in range are reduced when U_r/f^* is decreased,

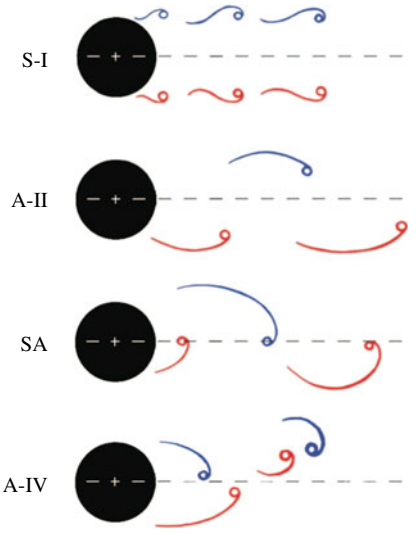

FIGURE 1. (Colour online) Sketch depicting the S-I, A-II, SA and A-IV modes, which occur in streamwise VIV. Flow is from left to right.

compared with when it is increased (Aguirre 1977). Within the second branch, the vortices are shed at half the cylinder vibration frequency ($f_{vs} = f_x/2$) and tend to form very close to the cylinder base (Aguirre 1977; Cagney & Balabani 2013*c*). Jauvtis & Williamson (2003) referred to this mode as the SA mode (see figure 1). This may be treated as a special case of the A-II mode. In the current work, the distinction between the A-II and SA modes is maintained to aid discussion.

Forced oscillation studies have shown that the wake can exhibit the A-IV mode (in which two pairs of counter-rotating vortices are shed per cycle; figure 1) at similar ranges of reduced velocity and vibration amplitude to that which are experienced by a cylinder in this region of the response regime (Ongoren & Rockwell 1988; Nishihara, Kaneko & Watanabe 2005; Konstantinidis, Balabani & Yianneskis 2007). Cagney & Balabani (2013*b*) showed that this mode can also occur in the wake of a freely vibrating cylinder; the mode was stable, and caused the second branch to occur in a slightly different form, with a lower-amplitude response compared with when the SA mode was present. At $U_r/f^* \approx 2.8$, the cylinder-wake system could appear in three different states; low-amplitude vibrations with the A-II mode occurring in the wake (when the reduced velocity was decreased); steady-state VIV when the A-IV mode occurred; and slightly larger amplitude VIV when the SA mode was present. It remains unclear what conditions influence the appearance of either mode, and whether these multiple stable states can occur for cylinders with multiple degrees of freedom. The latter question is important from a mathematical standpoint, as the number of possible stable states a system can exhibit is important in understanding and modelling its dynamics. It may also be of interest to the industrial engineer, as it raises the potential of using some form of active or passive control to restrict structures to the low-vibration states and thus reduce fatigue damage.

Relatively few studies investigating VIV of multi-DOF cylinders have examined the streamwise response regime, with most focusing on higher reduced velocity ranges, where the cylinder response occurs mostly in the transverse direction (Williamson & Jauvtis 2004; Flemming & Williamson 2005; Dahl *et al.* 2007; Sanchis *et al.* 2008).

Blevins & Coughran (2009) measured the amplitude response of a 2-DOF cylinder, which could also be constrained to move only in one direction. They found that the additional DOF did not substantially increase the amplitude response of the cylinder for $U_r/f^* \lesssim 4$ compared with the streamwise-only case. In the first branch they showed that the transverse response was negligible. This is consistent with the force-oscillation study of Nishihara *et al.* (2005), which showed that the S-I mode was dominant in this reduced velocity range, and induced a negligible lift force. Blevins and Coughran also showed that the cylinder followed a figure-of-eight trajectory in the second branch, with the frequency of the transverse oscillations equal to half the streamwise vibrations frequency. Jauvtis & Williamson (2003) showed that the S-I mode occurred in the first branch and the SA in the second. However, it should be noted that their study did not examine the variation in the wake mode throughout either branch, and it is unclear whether the A-II mode also occurred in the first branch, as in streamwise-only VIV.

1.2. *Aims of this work*

It is clear that there is a lack of information in the literature regarding VIV acting in the streamwise direction for bodies with multiple degrees of freedom. Several questions remain.

(*a*) What is the distribution of wake modes throughout the streamwise response regime and how does this compare with the 1-DOF case?
(*b*) Does mode competition between the S-I and A-II modes occur in the first response branch, and does this competition affect the transverse response of the cylinder?
(*c*) Does the additional DOF affect the number of possible states which can exist near $U_r/f^* \approx 2.8$? That is, can the second response branch appear in different forms, as found in streamwise-only VIV?
(*d*) How does the transverse motion of the cylinder affect the vortex-shedding process and vice versa?
(*e*) How do the cylinder trajectories vary throughout the streamwise response regime?

This paper aims to address these questions, and to extend the knowledge of the wake and structural dynamics associated with streamwise-only VIV to the more practical 2-DOF case. In particular, this paper follows recent work examining a cylinder free to move only in the streamwise direction for a moderate Reynolds number range (Cagney & Balabani 2013*c*,*a*,*b*). For the sake of brevity, these works are hereafter referred to as CB-1 (Cagney & Balabani 2013*c*), CB-2 (Cagney & Balabani 2013*a*) and CB-3 (Cagney & Balabani 2013*b*). In this paper, PIV measurements are presented of the wake and structural response at the centre-span of a 2-DOF cylinder undergoing VIV. The experiments described in this work were performed in the same test facility as previous studies (i.e. CB-1, CB-2, etc.). However, the current work examines a pivoted cylinder which was free to move in both the streamwise and transverse directions, rather than a cylinder which was supported with wires within the flow, such that it could only move in the streamwise direction.

2. Experimental details

The experiments were performed in a closed-loop water tunnel facility, which has been described in Konstantinidis, Balabani & Yianneskis (2003) and CB-1. The test section was made of Perspex to allow optical access, and had a cross-sectional area

of 72 mm × 72 mm. The flow was conditioned upstream using hexagonal honeycomb and a 9:1 contraction, such that the turbulence levels entering the test section were less than 2 % and the mean velocity was uniform to within 1 % 10 mm from the test-section walls. The flowrate was adjusted using mechanical valves, and the maximum freestream velocity in the test section was approximately 1 m s^{-1}. The temperature was held constant at $23 \pm 1\,^{\circ}\mathrm{C}$.

The use of a pivoted cylinder had significant advantages; its axisymmetric nature ensured that the natural frequency and damping were the same in both the streamwise and transverse directions, and it allowed the cylinder to be supported within the test section with minimal obstruction to the surrounding flow. VIV of pivoted or cantilevered cylinders in an interesting problem in its own right (King 1974; Fox & West 1993; Kitagawa *et al.* 1997; Balasubramanian *et al.* 2000; Fujarra *et al.* 2001; Nakamura *et al.* 2001; Okajima *et al.* 2001; Kitagawa *et al.* 2002; Okajima *et al.* 2002; Voorhees & Wei 2002; Flemming & Williamson 2005; Voorhees *et al.* 2008), and is relevant to structures such as marine piles, various biological flows (e.g. flow over vegetation and the whiskers of marine creatures; see Hanke *et al.* 2010; Levy & Liu 2013) and many structures which are subject to wind loading (e.g. chimneys and tall buildings). However, it should be noted from the offset that a pivoted cylinder is likely to have different dynamics compared with the two-dimensional cylinders (i.e. cylinders for which the amplitude response does not vary along their span) measured in CB-1, CB-2 and CB-3.

First, when the cylinder is pivoted, the motion is rotational, rather than translational, and the structural dynamics is controlled by the inertia ratio ($I^* = (\text{cylinder inertia})/(\text{inertia of the displaced fluid})$) rather than m^*. However, if the cylinder is solid (as in the current experiments), the two parameters are equivalent, $m^* = I^*$.

Second, the amplitude response of a pivoted cylinder will vary linearly along its span, which is likely to promote three-dimensional variations in the wake. Flemming & Williamson (2005) examined the wake modes along the span of a 2-DOF pivoted cylinder throughout the transverse response regime ($U_r/f^* \approx 4.5$–11) and found that when the inertia ratio was large, the 'quasi-uniform' assumption that the wake at each point along the span is the same as that which would occur for a two-dimensional cylinder oscillating at the same amplitude was valid. When I^* was lower, and the streamwise response was larger, the streamwise motion caused the wake to vary significantly from the case of a cylinder undergoing transverse-only VIV. However, their findings suggest that the pivoted nature of the cylinder does not significantly affect the fluid–structure interaction at a given point along the cylinder span, and the results presented in the following sections are relevant to the general case of multi-DOF cylinders undergoing VIV at low reduced velocities. The quasi-uniform assumption was also discussed by Techet, Hover & Triantafyllou (1998), who investigated the wake of a tapered cylinder forced to oscillate in the transverse directions. In this case, the variation in D caused the normalised amplitude response and the reduced velocity to vary linearly along the span. They found that the dominant wake mode at each point along the cylinder could be reasonably well predicted from the equivalent case of a two-dimensional cylinder at the same local values of A/D and reduced velocity (albeit with some variations due to Reynolds number effects), in agreement with the quasi-uniform assumption.

These studies suggest that in the absence of large variations in Re, etc., the quasi-uniform assumption is valid, which allows the measurements of the wake at a given plane along the cylinder span where the cylinder has a planar-amplitude, $A_x(z)$, to be compared with the wake of a two-dimensional cylinder vibrating at the same amplitude.

Direction	Mean value	Standard deviation
x	25.98 Hz	0.1 Hz
y	25.74 Hz	0.32 Hz

TABLE 1. Mean and standard deviations of the natural frequency of the cylinder in the streamwise and transverse directions, measured in still water. The values were calculated from a series of seven tests.

The cylinder had a diameter of 7.1 mm (figure 2), which matched that used in previous studies. The end of the cylinder was less than 0.5 mm from the test-section wall, which ensured that the free end was not associated with the formation of large, tip vortices, and the influence of the flow around the free end of the cylinder on the amplitude response was negligible (Morse & Williamson 2010). In order to ensure that the Reynolds number range ($Re = U_0 D/\nu$, where ν is the kinematic viscosity) in the current set of experiments was similar to that of the previous studies, the cylinder was required to have a relatively low natural frequency ($f_n \approx 15$–30 Hz). This required that the 'pin' connecting the pivoted cylinder to the test-section wall was relatively long, which caused the cylinder to have a relatively low aspect ratio, $AR = 8.45$. While this is undesirable, and may promote the influence of the end conditions on the cylinder response and flow measurements, it was decided to prioritise the similarity between the experimental conditions in the current and previous studies (i.e. D, Re, blockage ratio, etc.), at the expense of potentially increasing the influence of end effects on the measurements. This aspect ratio is also similar to that used in the streamwise VIV studies of Aguirre (1977), Nishihara *et al.* (2005) and the current authors (all $AR = 10$), and the 2-DOF study of Jauvtis & Williamson (2003) and Williamson & Jauvtis (2004) ($AR = 7.5$, 10). Further work is planned to examine the behaviour of cylinders of varying aspect ratios throughout the streamwise response regime; however, this is beyond the scope of the current work. The discussion of the results presented in the remainder of this manuscript is restricted to regions of the response regime which are consistent with the results of previous studies of two-dimensional cylinders, where the effects of the pivoted nature of the cylinder are expected to be negligible. Parameters that are likely to be significantly affected by the spanwise position (e.g. vortex strengths, Reynolds stresses etc.) are not examined.

The cylinder was made of solid aluminium, and had an inertia and mass ratio of 2.7. The natural frequencies and damping ratios of the cylinder were measured through a series of tap tests performed in air and water. The results of the natural frequency in water are summarised in table 1. The difference between the natural frequencies measured in the two directions are less than one standard deviation, and the two frequencies can be treated as being identical (as is the case for perfectly symmetrical structures). The natural frequency of the cylinder was thus taken as the mean of the values measured in both directions, $f_n = 25.86$ Hz.

The structural damping of the cylinder was estimated from tap tests performed in air (where the effects of fluid damping are considerably weaker than in water), the results of which are summarised in table 2. In this case the difference between the damping measured in both directions is only slightly larger than one standard deviation, and the damping is therefore also assumed to be approximately equal in both directions, with a mean value of $\zeta = 0.0039$.

The flow field surrounding the cylinder was measured using PIV. The plane normal to the cylinder axis at the centre-span of the larger-diameter cylinder (see

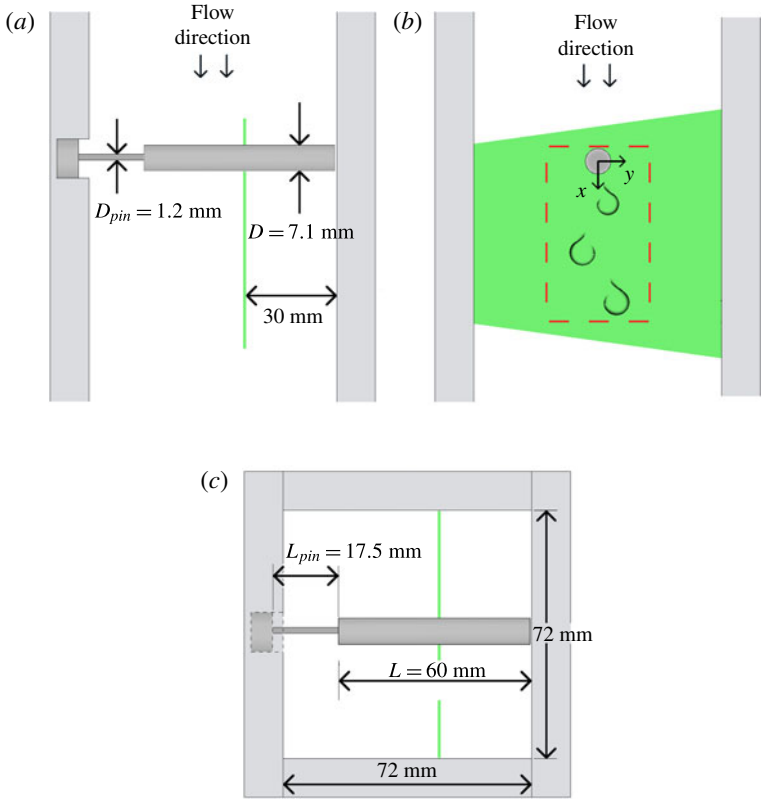

FIGURE 2. (Colour online) Elevation, side and plan view of the cylinder and test section, showing the position of the laser sheet and the origin of the coordinate system. The shaded (green online) areas indicate the position of the laser sheet and the dashed (red online) area indicates the PIV measurement domain.

figure 2) was illuminated using a continuous diode laser of 532 nm wavelength and a cylindrical lens, and images were acquired using an intensified CMOS camera. The images have a resolution of 876 pixel $\times$ 1280 pixel. The flow was seeded using silver-coated glass spheres, which had a mean diameter of 10 μm. PIV measurements were acquired throughout the reduced velocity range $U_r/f^* = 0.5$–3.5, which corresponded to a Reynolds number range of 675–5000. At each reduced velocity examined, 1000 image pairs were acquired at 200 Hz. After adjusting the freestream velocity, the flow was allowed to settle for at least 10 min before any measurements were acquired to reduce the influence of any transient effects. A mechanical traverse system was used to elevate the camera and laser system, and a series of PIV measurements of the flow entering the test section were acquired in order to measure the freestream velocity. The PIV system was then lowered, and measurements were acquired of the cylinder and wake. The velocity fields were calculated using a three-pass cross-correlation scheme with 50 % window overlap. The sizes of the initial and final interrogation windows were 32 $\times$ 32 and 12 $\times$ 12, respectively, and the final velocity fields had a spatial resolution of approximately 18 vectors per cylinder diameter. After each pass the normalised median test was applied, and erroneous vectors were replaced by their local median. As the cylinder was opaque, the region behind the cylinder was not illuminated in the PIV images,

Direction	Mean value	Standard deviation
x	0.0032	0.0005
y	0.0045	0.0012

TABLE 2. Mean and standard deviations of the damping ratio of the cylinder in the streamwise and transverse directions, measured in still air. The values were calculated from a series of five tests.

and no vectors could be calculated in this region. This shadow region was not present in previous studies performed in this test facility, as the cylinder in these cases was made of transparent Perspex.

The cylinder displacement signals in both directions were measured directly from the PIV images using a template-matching algorithm described in CB-1, which was found to be accurate to within 0.4 pixels ($\approx 0.002D$). In experimental studies of pivoted or cantilevered cylinders, it is typical to measure the amplitude at a single point along the span of the cylinder, e.g. Fujarra *et al.* (2001) and Flemming & Williamson (2005) measured the tip (maximum) amplitude, while Voorhees & Wei (2002) measured the amplitude at the centre-span of the cylinder. In this study we have adopted the latter approach, as the results are most likely to be representative of the 'average' flow along the cylinder span and therefore more likely to be comparable to the two-dimensional case examined in previous studies, and because the influence of end-effects are lowest at the centre-span (Kitagawa *et al.* 1997, 2002; Adaramola *et al.* 2006).

The mean of the cylinder displacement signals in both directions were used to define the spatial origin, and the PIV fields had a streamwise and transverse span of $x/D = -0.53$ to 5.78 and $y/D = -1.97$ to 2.01, respectively. The root-mean-square of the displacement signals was used to measure the response amplitude in both directions, A_x/D and A_y/D. These measures are representative of the overall amplitude response of the cylinder, which will in fact vary linearly along its span. The signals were first high-pass filtered with a cut-off frequency of 5 Hz, in order to reduce the influence of low-frequency fluctuations which are not associated with VIV. The cylinder response frequency was estimated using the maximum of the power spectra, calculated from the streamwise displacement signal.

The transverse velocity extracted from the PIV fields at $(x/D, y/D) = (3, 0.5)$ was used to estimate the vortex-shedding frequency, f_{vs}. Except where otherwise stated, this was also used as a reference signal to phase-average the velocity fields and cylinder displacement signals. The phase-averaged vorticity, $\langle \omega_z \rangle$ (where $\langle \cdot \rangle$ denotes a phase-averaged quantity) was calculated from the phase-averaged velocity fields. Spatial gradients were calculated using the least-squares method.

In order to increase the resolution of the measurements of the cylinder response regime without incurring prohibitive computational costs, additional measurements were acquired at certain flowrates in which only a small region in the vicinity of the cylinder was captured. For these measurements single images were acquired, rather than image pairs which could be used to perform PIV. For these measurements, 2000 images were acquired at 100 Hz, and were used only to estimate the cylinder displacement signals. This method was used to examine the amplitude response of the cylinder as the reduced velocity was decreased (i.e. to study the effects of hysteresis on the system) and to examine five additional reduced velocities as the flow rate was increased.

Property	Current study	CB-1, CB-3	CB-2
Re range	675–5000	450–3700	740–5400
U_r/f^* range	0.5–3.5	0.55–3.58	0.61–3.28
m^*	2.7	1.17	1.17
ζ	0.0039	0.0053	0.0037
f_n	27.54 Hz	15.08 Hz	23.7 Hz
AR	8.45	10	10
D	7.1 mm	7.1 mm	7.1 mm
Vector spacing	$18/D$	$15.5/D$	$18/D$

TABLE 3. Summary of the experimental conditions employed in the current work and previous studies. The vector spacing is the spatial resolution of the PIV measurements, expressed in terms of the number of vectors per cylinder diameter.

2.1. *Comparison with previous studies*

Throughout this paper, the results of the current set of experiments are compared with those found in previous studies examining a cylinder undergoing streamwise-only VIV. Experimental details for each case can be found in the relevant references; however, to assist the reader, table 3 summarises some of the relevant details regarding the flow and the cylinder properties.

Although effort was taken to ensure that the various experimental parameters were consistent across all three systems, there were some inevitable differences, particularly in the mass ratio and Re range, both of which will affect the amplitude response of the cylinder (Blevins & Coughran 2009). Along with the differences in the types of cylinders used (number of degrees of freedom pivoted, two-dimensional, etc.) this means that the magnitude of A/D is not directly comparable between studies.

3. Results

3.1. *Cylinder amplitude response*

The cylinder response amplitude of the pivoted cylinder in both the x and y directions is shown in figure 3(a), as well as the dominant frequency of transverse velocity fluctuations measured at $(x/D, y/D) = (3, 0.5)$ in figure 3(b). The response regime is characterised by two branches of approximately equal amplitude, as has been previously reported (CB-1; Aguirre (1977) and Okajima *et al.* (2003)).

The first response branch occurs in the range $U_r/f^* \approx 1.3$–2.45. The cylinder vibrations occur predominantly in the streamwise direction, with the levels of transverse motion remaining low, as observed in previous studies (Jauvtis & Williamson 2003; Blevins & Coughran 2009). Despite the presence of relatively large-amplitude streamwise vibrations, figure 3(b) shows that the velocity fluctuations three diameters downstream are not synchronised to the cylinder motion, and appear to follow the Strouhal relationship. This indicates that the symmetrically shed vortices have rearranged into an alternate pattern, as described in CB-2. The peak of the first response branch occurs at $U_r/f^* \approx 2.3$, at which point the frequency of the velocity fluctuations is equal to half the streamwise response frequency ($f_{vs}/f_x = 0.5$), indicating the onset of lock-in. This also coincides with an increase in A_y/D.

As the reduced velocity is increased further and $U_r/f^* \approx 2.5 \sim 1/2St$, the velocity fluctuations remain locked-in to $f_x/2$ and A_y/D continues to increase monotonically. However, the amplitude response in the streamwise direction falls slightly, which

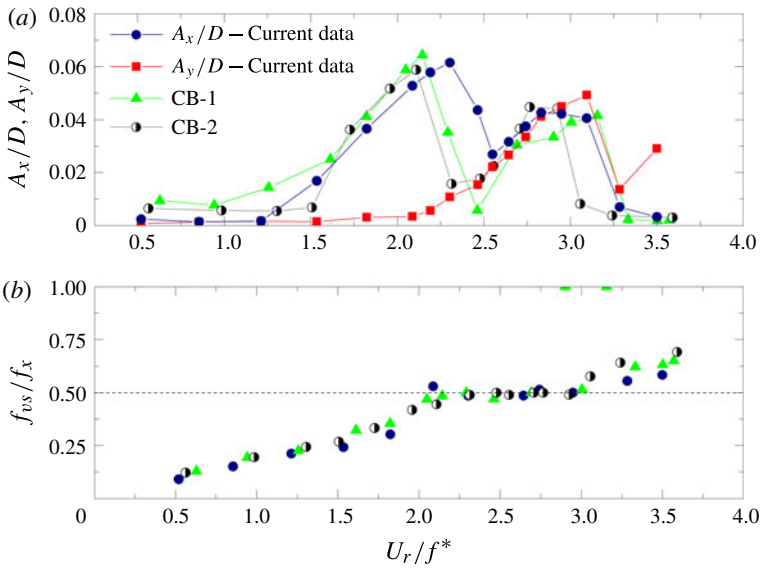

FIGURE 3. (Colour online) Variation in the streamwise and transverse amplitude response (*a*) and the dominant frequency of transverse velocity fluctuations at $(x/D, y/D) = (3, 0.5)$ (*b*) with reduced velocity. The results presented in CB-1 and CB-2 are also shown.

is characteristic of the streamwise VIV response regime (Aguirre (1977); Okajima *et al.* (2003); CB-1). Beyond this point the streamwise response amplitude begins to increase again as the cylinder enters the second branch. The amplitude in the transverse direction also continues to increase, and exceeds the streamwise amplitude at $U_r/f^* \approx 2.9$.

Finally at $U_r/f^* = 3.28$, the frequency of the velocity fluctuations in the wake are no longer locked-in to $f_x/2$, and the cylinder amplitudes in both directions fall. At higher reduced velocities, the transverse amplitude begins to increase again, which corresponds to the transverse response regime (Williamson & Jauvtis 2004).

The variations in the streamwise response amplitude and the frequency of velocity fluctuations in the wake observed in the present study are consistent with those found in CB-1 and CB-2 for the case of a single-DOF cylinder. However, there are some notable differences between the single- and 2-DOF cases; in particular, for the 2-DOF case the first response branch extends to a higher reduced velocity, and the vibrations are significantly larger at $U_r/f^* \approx 2.5$. Nakamura *et al.* (2001) examined the effects of the aspect ratio on the streamwise amplitude response of single-DOF, pivoted cylinders, and found that for $AR \lesssim 21$, the cylinder response regime did not exhibit a significant reduction in amplitude at $U_r/f^* \approx 2.5$; as AR was reduced further, the streamwise amplitude response at this point increased. Therefore, the comparatively large values of A_x/D observed in this region in figure 3 are likely to be associated with the choice of a relatively low aspect ratio ($AR = 8.45$) and the use of a pivoted cylinder.

Figure 4 presents the dominant wake mode observed throughout the response regime for each of the three sets of PIV measurements. The A-II mode tends to occur when the cylinder response is low, as the effect of the structural motion is not sufficient to alter the wake from the von Kármán vortex street observed behind stationary bodies. Both the alternate A-II and the symmetric S-I modes are observed

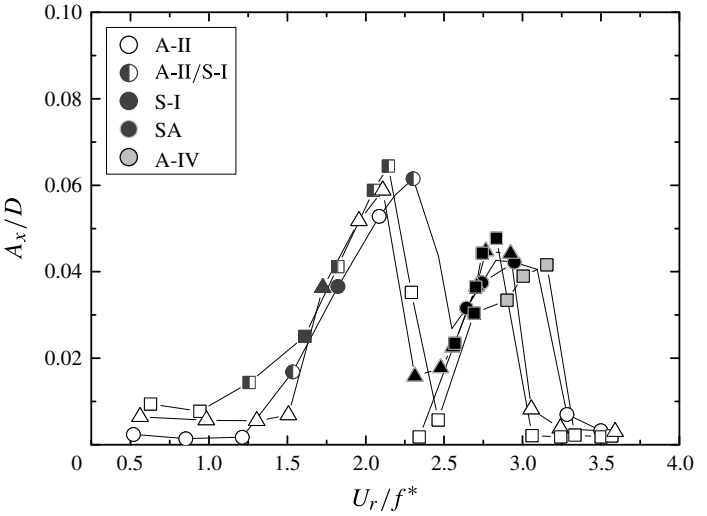

FIGURE 4. Streamwise response amplitude measured in the present study (circles), CB-1 (squares) and CB-2 (triangles). The colours indicate the dominant wake modes observed. Two-tone symbols indicate the points at which the wake was observed to switch between two different wake modes.

in the first branch, and at many points the two modes compete in an unsteady manner, without either mode being clearly dominant, as discussed in CB-2. It is notable that in all three cases, the A-II mode occurs at the peak of the first response branch. This is consistent with the early work of Aguirre (1977), but in contrast to the common assumption that the entirety of the first branch is associated only with symmetric vortex shedding (Okajima *et al.* 2003; Konstantinidis 2014). Figure 4 clearly shows that the first branch is caused by both alternate and symmetric shedding. The competition between these two forms of vortex shedding and its effect on the cylinder response is discussed in more detail in the following section.

The SA mode tends to dominate in the region of the second branch, when the vortex shedding is locked in to the cylinder motion. CB-3 showed that the wake can also exhibit the A-IV mode in this region (light grey squares in figure 4), although this mode was not observed in the current study. In general, the distribution of the wake modes observed in the current study is consistent with those observed for the previous single-DOF cases, with the exception of the occurrence of the SA mode at $U_r/f^* = 3.1$ and $A_x/D = 0.04$, which is likely to be caused by the presence of significant transverse cylinder motion. The effect of this transverse motion on the vortex-formation process and the dominant wake mode is discussed further in § 3.3.

3.2. *Effect of mode competition on transverse response*

It has been shown in a previous study (CB-2) that in the first response branch the wake alternates between the S-I and A-II wake modes. A mode-identification algorithm based on proper-orthogonal decomposition (POD) of the measured velocity fields was introduced to determine which mode is dominant in the wake of a single-DOF cylinder as a function of time. Analysis of the cylinder response at $U_r/f^* = 2.06$ indicated that the competition between the two modes did not have a significant effect on A_x/D. However, it was speculated that the mode competition may

affect a cylinder free to move in the transverse direction, as the alternate structure of the A-II mode is likely to induce an unsteady lift force. It is therefore interesting to examine the influence of both modes on the response of the pivoted cycle to test this hypothesis.

A detailed description of the mode-identification technique can be found elsewhere (CB-2) and is only briefly summarised here, while the reader is referred to Berkooz, Holmes & Lumley (1993) for a full description of the POD method. POD can be used to decompose a set of N velocity fields into N orthogonal spatial modes, $\boldsymbol{\Phi}_i(x, y)$ (where $i = 1, 2 \ldots N$), each of which has a temporal coefficient $a_i(t)$. The flow field can then be expressed as

$$\boldsymbol{U}(x, y, t) = \overline{\boldsymbol{U}}(x, y) + \sum_{i=1}^{N} a_i(t)\boldsymbol{\Phi}_i(x, y), \tag{3.1}$$

where $\boldsymbol{U}$ is the velocity field (containing all measured components) and $\overline{\boldsymbol{U}}$ is the mean velocity field.

For flows which are dominated by vortex shedding, the first two POD modes will occur as a pair which are 90° out of phase, and will capture the shedding process (van Oudheusden *et al.* 2005). When there is significant mode competition in the wake, the first two POD modes will correspond to the primary shedding mode, while the third and fourth POD modes will correspond to the secondary shedding pattern. The dominance of either wake mode at a given time can be estimated from the instantaneous amplitude of the POD coefficients (calculated using the Hilbert transform), $\mathscr{H}(a_i(t))$. This can be used to determine which wake mode is present at a given time: if

$$\mathscr{H}(a_1(t)) + \mathscr{H}(a_2(t)) > \mathscr{H}(a_3(t)) + \mathscr{H}(a_4(t)) \tag{3.2}$$

then the primary mode (corresponding to POD modes 1 and 2) is said to be dominant, while the secondary mode dominates when this condition is not met.

This method has successfully been used to compute two sets of phase-averaged velocity fields for both the S-I and A-II wake modes using the same set of PIV measurements and the same reference signal (i.e. the only difference between the computation of the two sets of averaged fields was the criterion in (3.2)); see figure 5 in CB-2.

Before applying this method to the current set of measurements, it is worth making a note on the nature of the mode-identification technique and mode competition in general. The wake modes in VIV are defined based on visual examination of the flow (Ongoren & Rockwell 1988; Williamson & Roshko 1988), and are therefore an inherently qualitative description. This is especially true when the modes vary with time. Therefore, the effectiveness of any mode-identification technique cannot be said to have a quantifiable accuracy, and the criterion defined above should not be thought of as a quantitative or Boolean measure of the wake mode present at a given instant, but rather as a means of providing a qualitative measure.

In order to confirm that the criterion is effective, it is first necessary to show that it can be used to isolate phase-averaged vorticity fields corresponding to both wake modes using the same set of measurements and reference signal. This is outlined below for the PIV measurements acquired in the wake of the pivoted cylinder at $U_r/f^* = 2.09$.

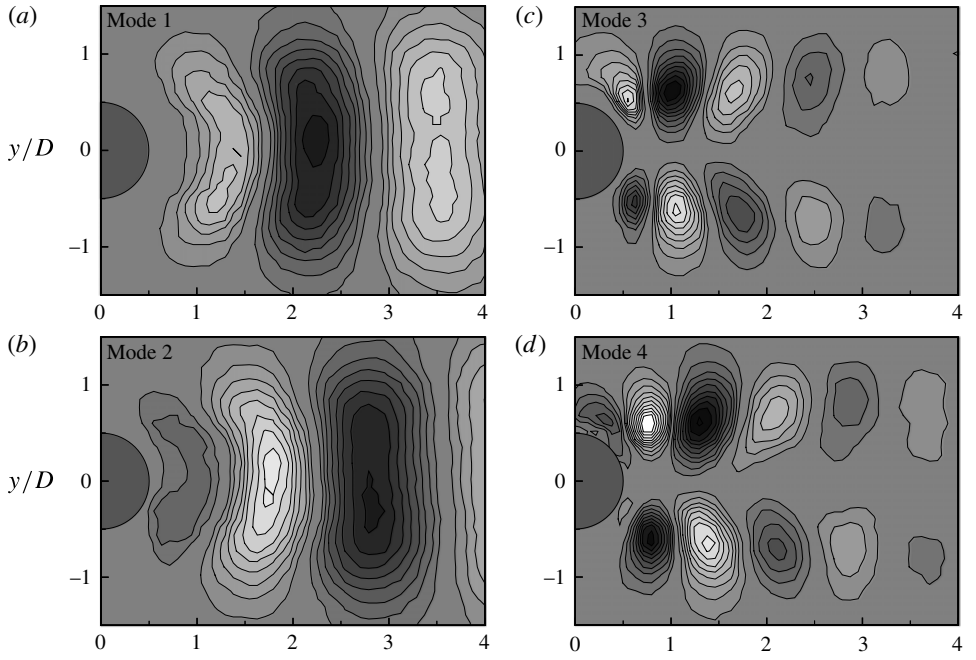

FIGURE 5. Transverse velocity fields for POD modes 1–4 (*a–d*) for $U_r/f^* = 2.09$. The scales are arbitrary.

POD was performed for the velocity measurements in the region $x/D = 0$–4. The first two POD modes were found to correspond to the A-II mode (figure 5*a*,*b*), while the third and fourth POD modes were found to correspond to S-I mode (figure 5*c*,*d*). The respective amplitude coefficients ($a_1(t)$, $a_2(t)$, etc.) were also found to occur in pairs, which were 90° out of phase. This indicates that the A-II mode is the most energetic (i.e. dominant), and the S-I mode is a secondary feature, occurring in a smaller number of PIV fields.

Figure 6 shows the phase-averaged vorticity fields and cylinder displacement signals calculated for both modes using the transverse velocity signal measured at $(x/D, y/D) = (2, 0.5)$ and the mode-identification criterion. Although the vorticity fields are in some cases quite disorganised, the characteristic symmetric and alternate wake structures are both apparent; two rows of counter-rotating vortices are present in figure 6(*f*) at $x/D \approx 1$ and 2, when the S-I mode is dominant, while the vortices are clearly arranged in an alternate pattern when the A-II mode occurs ($x/D \approx 1$–4 in figure 6*a–d*). Likewise, the phase-averaged displacement signals show characteristic differences; the signal $\langle x/D \rangle$ in figure 6(*e*) occurs at twice the frequency of the velocity fluctuations in the wake, while in figure 6(*j*) it occurs at the same frequency as the fluctuations. This is consistent with the known behaviour of the A-II and S-I modes, respectively (CB-1, CB-2).

Both sets of fields contain some signs of 'contamination'; some symmetric features are present in the A-II vorticity fields (figure 6*a–d*), indicating that some instantaneous fields in which the S-I mode is present have been used to calculate the phase-averaged fields for the A-II mode (and vice versa). Similarly, the phase-averaged streamwise displacement signal in figure 6(*e*) occurs at twice the reference signal ($f_{vs} = f_x/2$), but the two peaks in figure 6(*e*) are not equal height, with the peak at $t/T = 15/16$ slightly

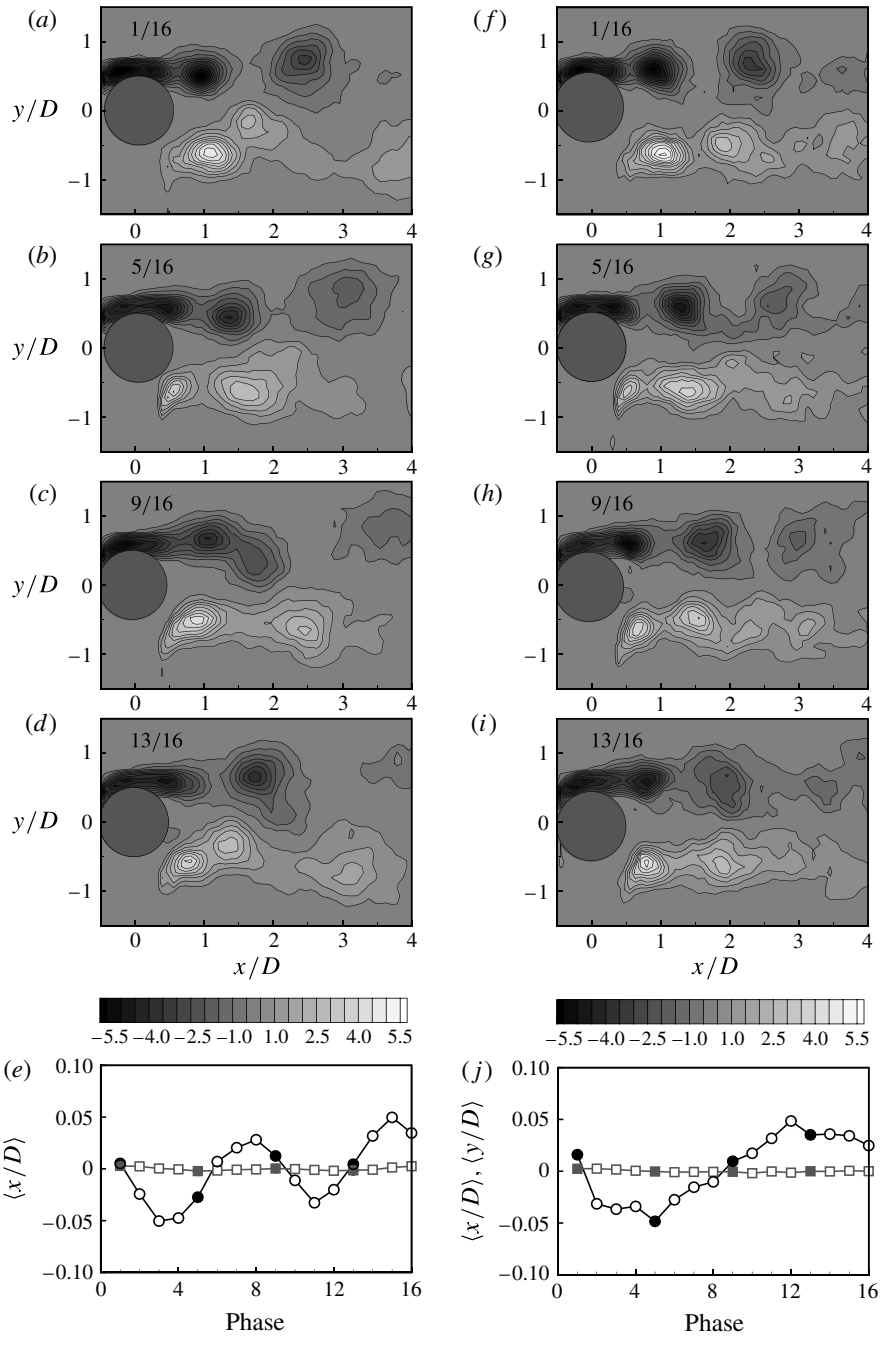

FIGURE 6. Phase-averaged vorticity fields computed at $U_r/f^* = 2.09$, showing the A-II (*a–d*) and the S-I mode (*f–i*). The associated phase-averaged displacement signals are shown in (*e*) and (*j*), respectively. Both sets of average fields and displacement signals were calculated from the same set of PIV measurements and using the same reference signal, and were differentiated using the mode-identification technique described in CB-2.

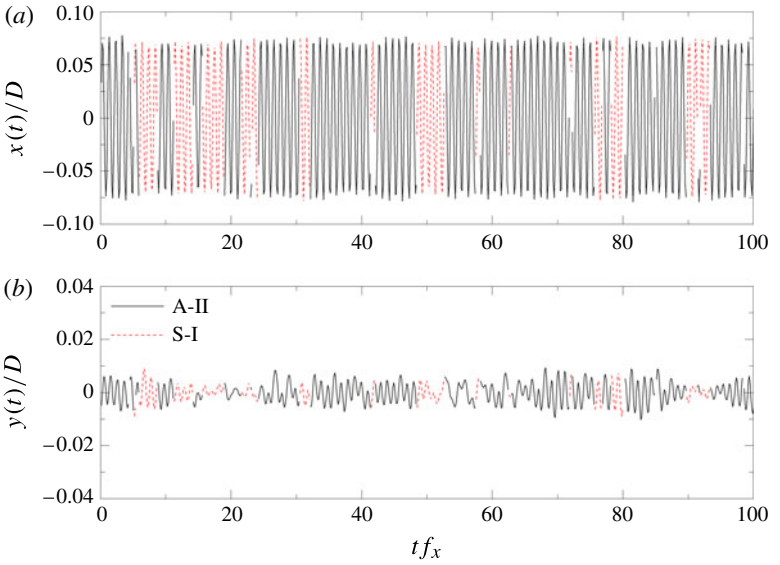

FIGURE 7. (Colour online) Cylinder displacement signals in the streamwise (*a*) and transverse (*b*) directions, measured at $U_r/f^* = 2.09$. The symbol colours denote which mode was determined to be present in the wake; A-II (black), S-I (dashed (red online)).

larger than the earlier peak. This suggests that the phase-averaged displacement signal contains a weak subharmonic component at the symmetric vortex-shedding frequency ($f_{vs} = f_x$), i.e. the signal has been contaminated. However, in general, the phase-averaged vorticity fields and displacement signals capture the characteristic features associated with both wake modes, and the mode-identification technique can be said to provide an effective (albeit qualitative) means of determining which mode is dominant as a function of time.

The cylinder displacement signals measured in the streamwise and transverse directions at this reduced velocity are shown in figure 7(*a*,*b*), respectively. The symbol colours denote which wake mode was identified as dominant at each instant. Both wake modes appear to provide the same levels of fluid excitation to the cylinder, as the amplitude of the streamwise displacement signal appears to be unaffected by the occurrence of either mode. This is consistent with what was found for the 1-DOF case (CB-2). In spite of the alternate nature of the A-II mode (which might be expected to cause this mode to induce an unsteady lift force), the presence of either the S-I or A-II mode does not appear to affect the amplitude of the cylinder vibration in the transverse direction. Nor was the intermittent appearance of either mode found to have a noticeable effect on the transverse displacement signal measured at any reduced velocity in the first response branch.

It is unclear why the appearance of the A-II mode at the peak of the first response branch coincides with a significant increase in A_y/D (figure 4), but the mode does not appear to affect $y(t)/D$ when it occurs intermittently. A potential explanation is that the mode competition is highly three-dimensional, and the dominant wake mode varies along the cylinder span, i.e. at a given instant both the A-II and S-I modes exist simultaneously at different points along the span. If this is the case, it is not the wake mode and sectional fluid forces in a single plane (e.g. the PIV plane shown here) which affect the amplitude response of the cylinder, but the fluid forces integrated over

Study	U_r/f^*	A_x/D	A_y/D	Re
CB-2 (1-DOF)	2.92	0.044	0	4160
Current study (2-DOF)	2.95	0.042	0.045	4180

TABLE 4. Experimental details associated with the PIV measurements of a 1- and 2-DOF cylinder, in which the SA mode was observed in the wake.

the entire span, and the mode competition at a given plane will have little effect on the overall fluid forcing. To fully examine this hypothesis would require the use of a 3D flow measurement technique such as tomographic PIV or 3D numerical simulations.

In summary, it appears that this competition does not have a significant effect on the cylinder excitation in either direction, and that the wake dynamics and fluid–structure interaction in the first response branch are not significantly affected by the additional DOF of the cylinder. Therefore, the results of various studies of streamwise-only VIV in this reduced velocity range are likely to remain relevant to the more practical, multi-DOF case.

3.3. *Effect of y-motion on the wake modes in the second branch*

Figure 4 shows that the SA mode is observed at approximately the same values of A_x/D and U_r/f^* for both the 1- and 2-DOF cylinders. The vorticity fields measured in both cases can be compared, allowing the effects of the transverse cylinder motion on the vortex formation process to be identified.

Two sets of PIV measurements acquired at $U_r/f^* \approx 2.9$ for a single- and 2-DOF cylinder were compared. Some details of these measurements are summarised in table 4. The velocity fields and cylinder displacement signals were phase-averaged for both cases, as described in § 2. The resulting vorticity fields at four phases are shown in figure 8(*a–d*) for the 1-DOF case, along with the corresponding streamwise displacement signal in figure 8(*e*). The vortex-shedding cycle associated with the SA wake mode has been described in detail elsewhere (CB-1), and therefore only a brief summary is provided here.

As the cylinder is in its most downstream position, a negative vortex has formed near the cylinder base, at approximately $x/D = 1$ in figure 8(*a*). The cylinder then moves upstream (figure 8*b*), causing vorticity of the opposite sign to be entrained into the region of the near wake which the cylinder has recently vacated; as the cylinder reaches its peak upstream position (figure 8*c*), this positive vorticity at the cylinder base begins to roll up to form a new vortex. This vortex remains attached to the cylinder as it again moves downstream (figure 8*d*), and will be shed as the cylinder reaches its peak downstream position and the cycle repeats for a vortex of the opposite sign.

The corresponding vorticity fields and cylinder displacement signals for the 2-DOF cylinder at approximately the same reduced velocity are shown in figure 8(*f–j*). The magnitude of the vorticity in the 2-DOF case is lower than that shown in figure 8(*a–d*). This difference in magnitude was also apparent in the instantaneous fields, and cannot be attributed to the phase-averaging process (as could happen, for example, if the reference signal was only weakly correlated to the vortex-shedding process in the 2-DOF case). Therefore, it appears that the additional transverse motion of the cylinder acts to decrease the amount of vorticity created throughout each shedding cycle. However, it should be noted that the results presented in

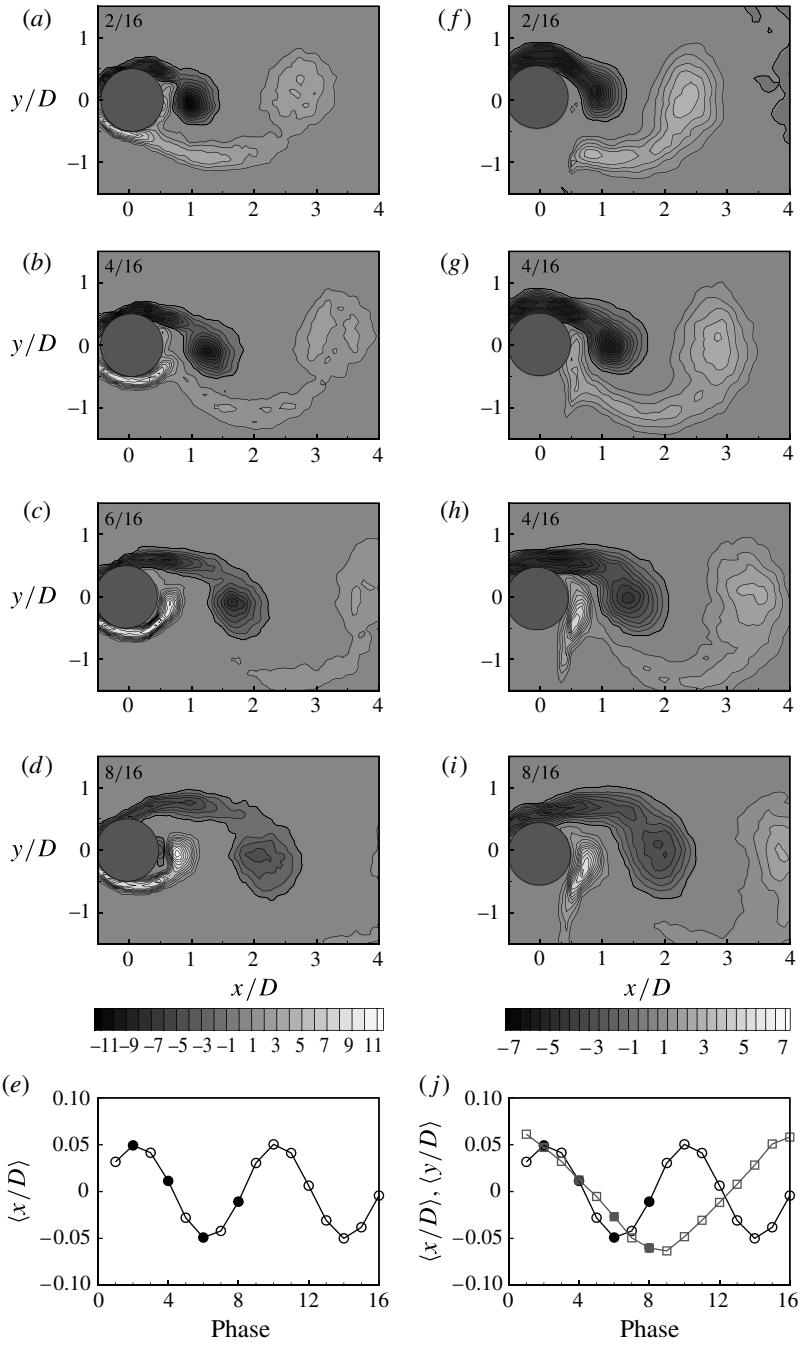

FIGURE 8. Phase-averaged vorticity fields and displacement signals for the 1-DOF (*a–e*) and 2-DOF (*f–i*) cylinders. The vorticity fields represent half a shedding cycle, while the SA mode is dominant in the wake. The circles in (*e*) and (*i*) represent the phase-averaged streamwise displacement, while the squares in (*i*) indicate the transverse values. The closed symbols correspond to the phases shown in (*a–d*) and (*f–i*). Some details of the experimental conditions for both cases are listed in table 4.

figure 8(*a–d*) and (*f–i*) were acquired using different PIV systems; as PIV measurements act as a low-pass filter on the true velocity field and tend to reduce the estimates of vorticity (Stanislas, Okamoto & Kähler 2003), this reduction in $\langle\omega_z\rangle$ may in part be attributable to the different experimental systems.

In spite of this difference, the vortex-shedding processes for both cases appear to be remarkably similar. This suggests that the ability of the cylinder to move normal to the flow does not have a significant effect on the vortex-shedding process.

However, the additional DOF affects the cylinder-wake system in other ways. Figure 4 indicates that for the 1-DOF case, the A-IV mode occurs in the wake at $U_r/f^* \approx 3$ and $A_x/D \approx 0.04$, while the SA mode is observed for 2-DOF cylinder at a similar point in the $U_r/f^* - A_x/D$ plane. Thus, the transverse motion of the cylinder appears to change the dominant wake mode, which in turn is also likely to alter the fluid forces, levels of energy transfer to the structure, the added mass, etc. A similar effect has also been noted for the case of transverse VIV; Morse & Williamson (2009) showed that the wake mode of a cylinder oscillating in the transverse direction can be accurately predicted if the reduced velocity and vibration amplitude are known. However, when the cylinder is free to move in the two directions, the wake mode becomes a function of the reduced velocity and the vibration amplitude in both directions (Flemming & Williamson 2005). The distribution of wake modes presented in figure 4 suggest that this is also the case at low reduced velocities ($U_r/f^* \approx 3$), when the cylinder response is controlled by the streamwise excitation.

The results presented in CB-3 showed that when the cylinder is free to move only in the streamwise direction, the cylinder-wake system can exhibit three possible states in the region of the second branch, in which either the SA, A-IV or A-II modes occur in the wake, with each mode corresponding to a distinct level of cylinder excitation and amplitude response. For the 1-DOF case, the A-II mode was observed when the reduced velocity was decreased from an initially high value and the cylinder response was negligible (i.e. the extent of the second branch was considerably smaller due to hysteresis effects), as can be seen in figure 9(*a*), which shows the three possible forms of the second response branch. However, for the 2-DOF case, the freedom to move in the transverse direction appears to prevent the occurrence of the A-IV mode. Therefore, the wake can only exhibit one wake mode in this region (the SA mode) and only one form of the second response branch occurs. Consequently the streamwise response regime is unaffected by hysteresis.

While there are three possible cylinder-wake states which can occur in the region of the second response branch for the streamwise-only case of VIV, it appears that the ability of the cylinder to move in the transverse direction results in only one favourable state existing (i.e. non-negligible cylinder vibration with the SA mode occurring in the wake). Although the phase-averaged vorticity fields in figure 8 suggest that the transverse motion of the cylinder does not significantly alter the vortex-formation process when the SA mode is dominant, the additional DOF has important implications for the overall cylinder–wake system, altering the distribution of wake modes throughout the response regime, the streamwise vibration amplitude and the effects of hysteresis on the system.

3.4. *Cylinder trajectories*

Figure 10(*a–h*) shows the x and y trajectories of the cylinder in the reduced velocity range $U_r/f^* = 2.3$–3.1. This corresponds to the lock-in range, i.e. the peak of the first response branch, the low-amplitude region at $U_r/f^* \approx 2.5$ and the second response

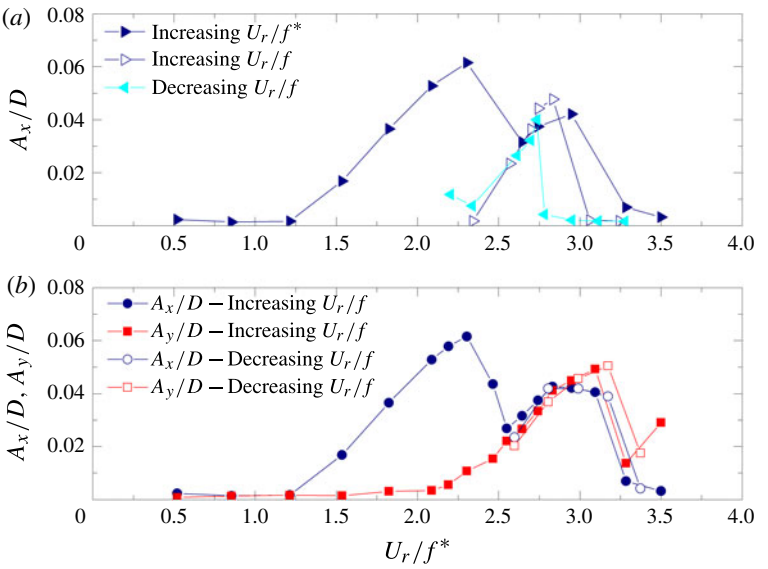

FIGURE 9. (Colour online) The amplitude response as the reduced velocity is incrementally increased and decreased, for the various states of the 1-DOF cylinder examined in CB-2 (*a*) and for the 2-DOF cylinder (*b*). While the cylinder-wake system can exhibit one of three possible states in the region $U_r/f^* \approx 2.5$–3.5 for the 1-DOF case, the 2-DOF cylinder is not affected by hysteresis and only exhibits one state in this region.

branch. The alternate vortex shedding observed at the peak of the first branch causes the cylinder to vibrate in the transverse direction at $f_x/2$; this can be seen in figure 10(*a*), as the cylinder appears to follow a figure-of-eight trajectory. The figure-of-eight pattern appears to be characteristic of VIV, and has been observed in a number of studies of multi-DOF cylinders (Dahl *et al.* 2007; Sanchis *et al.* 2008; Blevins & Coughran 2009; Horowitz & Williamson 2010). This pattern becomes more pronounced as the reduced velocity and A_y/D increase (figure 10*b–h*); at $U_r/f^* = 2.3$ the pattern is strongly asymmetrical about the line $x/D = 0$, but becomes increasing symmetrical as U_r/f^* increases. The changes in the x–y path with increasing reduced velocity is caused by a change in the phase angle between the x and y motion, ϕ_{xy}.

In order to quantify this change in phase, the displacement signals were modelled as

$$x(t) = B_x \sin(2\pi f_x t + \phi_x), \tag{3.3}$$

$$y(t) = B_y \sin\left(\pi f_x t + \phi_y\right), \tag{3.4}$$

where B_b, B_y, ϕ_x and ϕ_y are constants which could be found empirically from the displacement signals. This was achieved by first phase-averaging both the x and y signals with respect to the y signal itself, in order to reduce the influence of measurement noise and low-frequency variations in the amplitudes of this signals, and then fitting the averaged values to (3.3) and (3.4) using a least-squares approach. The phase-averaged values and the fitted signals are also shown in figure 10. Equations (3.3) and (3.4) can then be rearranged as

$$x(t) = B_x \sin\left(2\pi f_x t + \phi_{xy}\right), \tag{3.5}$$

$$y(t) = B_y \sin(\pi f_x t), \tag{3.6}$$

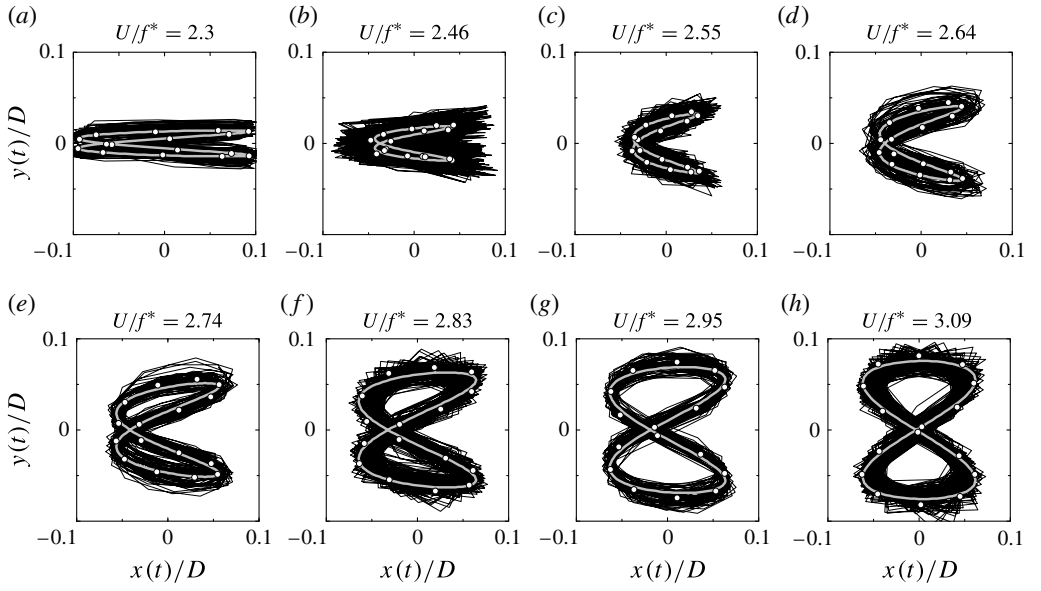

FIGURE 10. The x–y trajectories followed by the cylinder in the reduced velocity range $U_r/f^* = 2.3$–3.1. The black lines indicate the raw displacement signals, while the white symbols indicate the phase-averaged x and y positions (which were averaged with respect to the y motion) and the thick grey line is a sine-wave fit to the phase-averaged data.

where

$$\phi_{xy} = \phi_x - 2\phi_y. \tag{3.7}$$

The variation in the estimated values of ϕ_{xy} with reduced velocity is shown in figure 11(*b*). The phase lag decreases steadily with U_r/f^* throughout the lock-in range. There is a sudden jump of -0.29π between $U_r/f^* = 2.46$ and 2.55, which coincides with a change in the vortex-formation process in this region, as the SA mode becomes dominant. When the SA mode is dominant ($U_r/f^* = 2.55$–3.09), the phase lag between the x and y motion decreases in an approximately linear manner. At the highest reduced velocity at which lock-in occurs, the phase lag approaches $-\pi$; beyond this point the amplitudes in both directions decrease, the displacement signals become unsteady and ϕ_{xy} can no longer easily be defined.

In order to investigate the cause of this change in phase throughout the lock-in range, the PIV measurements of the cylinder wake were examined. The x and y positions of the cylinder and the velocity fields were phase-averaging with respect to the transverse velocity signal measured at $(x/D, y/D) = (3, 0.5)$. Figure 12(*a–c*) shows the resulting phase-averaged vorticity fields as the cylinder is in its most downstream position throughout the region $U_r/f^* = 2.3$–2.95, while the corresponding cylinder displacement signals are shown in figure 12(*d–f*).

One might reasonably expect the change in ϕ_{xy} to be accompanied by a change in the phase of the vortex shedding with respect to the streamwise motion. However, examination of the vorticity fields in figure 12 (as the cylinder is in its most downstream position) do not reveal any such behaviour. In each case, a negative vortex is forming at the cylinder base, while a recently shed positive vortex is present at $x/D \approx 2$. This vortex appears slightly further downstream at higher reduced

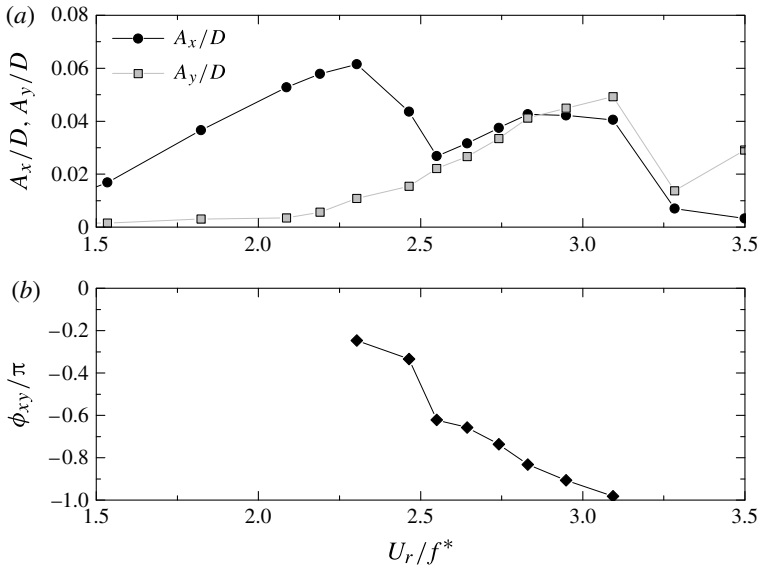

FIGURE 11. Variation in the amplitude response of the cylinder in the streamwise (circles) and transverse (grey squares) directions (*a*) and the phase angle between the streamwise and transverse motion (*b*).

velocities; however, this is caused by an increase in the wavelength of the wake, $\lambda_{wake} \propto U_0/f_{vs} = 2U_0/f_x = 2DU_r/f^*$, rather than a change in the phase of the shedding.

The absence of a significant change in the phase of the vortex shedding is consistent with the work of Jeon & Gharib (2001), who forced a cylinder to oscillate in both the streamwise and transverse directions at peak non-dimensional amplitudes of 0.1 and 0.5, respectively; the vibration frequencies were varied such that $f_x/f_y = 2$ and $\phi_{xy} = 0$ and $-\pi/4$ (and $U_r/f^* = 4$ and 6). They found that the transverse motion controlled the vortex-shedding frequency, while the streamwise motion controlled its phase. In the vorticity fields shown in figure 12, it is the streamwise motion which controls the shedding frequency (since the cylinder is in the streamwise rather than the transverse response regime, i.e. $U_r/f^* \sim 1/2St$, rather than $1/St$), but it appears that in both cases the phase of the shedding is determined by the streamwise motion.

This work demonstrates some of the similarities and differences between the structural response and wake dynamics of single- and 2-DOF cylinders in the streamwise response regime. Further work is required to identify the influence of the pivoted nature of the cylinder, e.g. the effects of the aspect ratio and the three-dimensionality in the wake. However, the results presented here indicate that much of the knowledge of streamwise VIV of 1-DOF cylinders may be extended to the multi-DOF case, with the exception of the region of the second response branch, where the additional DOF appears to simplify the dynamics of the system, reducing the number of possible states.

4. Conclusions

The structural response and wake dynamics of a pivoted 2-DOF cylinder have been measured throughout the streamwise response regime ($U_r/f^* \lesssim 4$) using PIV. The results have been compared with studies performed in the same water tunnel facility

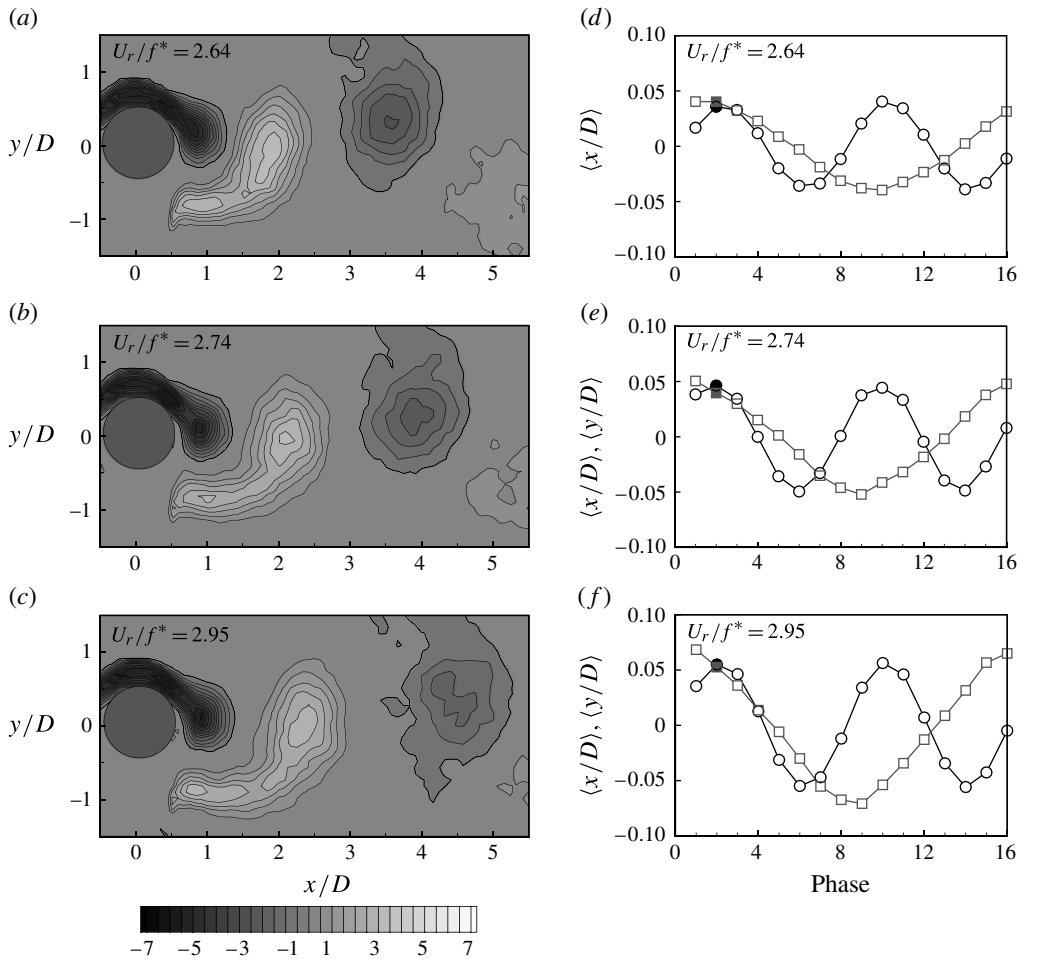

FIGURE 12. Phase-averaged vorticity fields (*a–c*) and the corresponding streamwise displacement signal (*d–f*) at three points in the second response branch. The closed symbols in (*d–f*) indicate the phase shown in (*a–c*). The vorticity fields do not indicate that the phase of vortex shedding varies throughout this reduced velocity range.

using a cylinder free to move only in the streamwise direction at a similar range of reduced velocity and Reynolds number.

The response regime in both cases was similar, containing two branches, separated by a region of low-amplitude response at $U_r/f^* \approx 2.5$, in agreement with various studies in the literature. Within the first branch, the wake exhibited both the S-I and A-II modes, and the vibrations occurred predominantly in the streamwise direction. However, the transverse amplitude response increased as the A-II mode became dominant near the maximum of the branch. The wake in both the 1- and 2-DOF cases was found to switch intermittently between the two modes at certain points within this branch. In both cases, this mode competition was not found to affect the cylinder response amplitude in either direction. In general the results for the 1- and 2-DOF cases in this region of the response regime were in good agreement, suggesting that much of the results in the literature concerning VIV of single-DOF cylinders in this region can be extended to the multi-DOF case.

For the 1-DOF case, the second branch is capable of existing in three distinct forms, which are associated with three different wake modes at $U_r/f^* \approx 2.8$. However, while the freedom of the cylinder to move in the transverse direction was found to have little effect on the vortex-shedding process when the SA mode dominated in this region, the additional DOF had a significant effect on the response regime; the cylinder response was no longer hysteretic, the A-IV mode was not observed and the second branch appeared in only one form. This indicates that the additional DOF has a significant effect on the overall dynamics of the cylinder–wake system. By reducing the number of possible states that the cylinder can occupy in this region, the extra DOF appears to simplify the overall dynamics, rather than making the fluid–structure interaction problem more complex.

When the cylinder experienced significant transverse vibrations, from the peak of the first branch to the end of the second branch ($U_r/f^* = 2.3$–3.1), the cylinder followed figure-of-eight trajectories. The phase angle between the streamwise and transverse displacement signals was found to decrease in a linear manner with reduced velocity, with a sudden jump when the wake changed from the A-II to the SA mode. Examination of the phase-averaged vorticity fields acquired in the second response branch indicated that this change in phase did not coincide with a change in the phase of vortex shedding with respect to the streamwise motion, which remained constant.

REFERENCES

ADARAMOLA, M. S., AKINLADE, O. G., SUMNER, D., BERGSTROM, D. J. & SCHENSTEAD, A. J. 2006 Turbulent wake of a finite circular cylinder of small aspect ratio. *J. Fluids Struct.* **22**, 919–928.

AGUIRRE, J. E. 1977 Flow induced, in-line vibrations of a circular cylinder. PhD thesis, Imperial College of Science and Technology.

BALASUBRAMANIAN, S., SKOP, R. A., HAAN, F. K. JR & SZEWCYZK, A. A. 2000 Vortex-excited vibrations of uniform pivoted cylinders in uniform and shear flow. *J. Fluids Struct.* **14**, 64–85.

BEARMAN, P. W. 1984 Vortex shedding from oscillating bluff bodies. *Annu. Rev. Fluid Mech.* **16**, 195–222.

BERKOOZ, G., HOLMES, P. & LUMLEY, L. 1993 The Proper Orthogonal Decomposition in the analysis of turbulent flows. *Annu. Rev. Fluid Mech.* **25**, 539–575.

BLEVINS, R. D. & COUGHRAN, C. S. 2009 Experimental investigation of vortex-induced vibrations in one and two dimensions with variable mass, damping, and Reynolds number. *Trans. ASME J. Fluids Engng* **131** (101202), 1–7.

CAGNEY, N. & BALABANI, S. 2013*a* Mode competition in streamwise-only vortex induced vibrations. *J. Fluids Struct.* **41**, 156–165.

CAGNEY, N. & BALABANI, S. 2013*b* On multiple manifestations of the second response branch in streamwise vortex-induced vibrations. *Phys. Fluids* **25**, 075110.

CAGNEY, N. & BALABANI, S. 2013*c* Wake modes of a cylinder undergoing free streamwise vortex-induced vibrations. *J. Fluids Struct.* **38**, 127–145.

DAHL, J. M., HOVER, F. S., TRIANTAFYLLOU, M. S., DONG, S. & KARNIADAKIS, G. E. 2007 Resonant vibrations of bluff bodies cause multivortex shedding and high frequency forces. *Phys. Rev. Lett.* **99**, 144503.

DAHL, J. M., HOVER, F. S., TRIANTAFYLLOU, M. S. & OAKLEY, O. H. 2010 Dual resonance in vortex-induced vibrations at subcritical and supercritical Reynolds numbers. *J. Fluid Mech.* **643**, 395–424.

FENG, C. C. 1963 The measure ment of vortex induced effects in flow past stationary and oscillating circular and d-section cylinders. Master's thesis, The University of British Columbia, Department of Mechanical Engineering.

FLEMMING, F. & WILLIAMSON, C. H. K. 2005 Vortex-induced vibrations of a pivoted cylinder. *J. Fluid Mech.* **552**, 215–252.

FOX, T. A. & WEST, G. S. 1993 Fluid-induced loading of cantilevered circular cylinders in a low-turbulence unform flow. Part 2: fluctuating loads on a cantilever of aspect ratio 30. *J. Fluids Struct.* **7**, 15–28.

FUJARRA, A. L. C., PESCE, C. P., FLEMMING, F. & WILLIAMSON, C. H. K. 2001 Vortex-induced vibrations of a flexible cantilever. *J. Fluids Struct.* **15**, 651–658.

GOVARDHAN, R. & WILLIAMSON, C. H. K. 2000 Modes of vortex formation and frequency response of a freely vibrating cylinder. *J. Fluid Mech.* **420**, 85–130.

GOVARDHAN, R. & WILLIAMSON, C. H. K. 2002 Resonance forever: existence of a critical mass and an infinite regime of resonance in vortex-induced vibration. *J. Fluid Mech.* **473**, 147–166.

GRIFFIN, O. M. & RAMBERG, S. E. 1976 Vortex shedding from a cylinder vibrating in line with an incident uniform flow. *J. Fluid Mech.* **75**, 257–271.

HANKE, W., WITTE, M., MIERSCH, L., BREDE, M., OEFFNER, J., MICHAEL, M., HANKE, F., LEDER, E. & DEHNHARDT, G. 2010 Harbor seal vibrissa morphology suppresses vortex-induced vibrations. *J. Expl Biol.* **213**, 2665–2672.

HOROWITZ, M. & WILLIAMSON, C. H. K. 2010 Vortex-induced vibration of a rising and falling cylinder. *J. Fluid Mech.* **660**, 1–32.

JAUVTIS, N. & WILLIAMSON, C. H. K. 2003 Vortex-induced vibration of a cylinder with two degrees of freedom. *J. Fluids Struct.* **17**, 1035–1042.

JEON, D. & GHARIB, M. 2001 On circular cylinders undergoing two-degrees-of-freedom forced motions. *J. Fluids Struct.* **15**, 533–541.

KHALAK, A. & WILLIAMSON, C. H. K. 1999 Motions, forces and mode transitions in vortex-induced vibrations at low mass-damping. *J. Fluids Struct.* **13**, 813–851.

KING, R. 1974 Vortex excited structural oscillations of a circular cylinder in flowing water. PhD thesis, Loughborough University of Technology.

KITAGAWA, T., FUJINO, Y., KIMURA, K. & MIZUNO, Y. 2002 Wind pressures measurement on end-cell-induced vibration of a cantilevered circular cylinder. *J. Wind Engng Ind. Aerodyn.* **90**, 395–405.

KITAGAWA, T., WAKAHARA, T., FUJINO, Y. & KIMURA, K. 1997 An experimental study on vortex-induced vibration of a circular cylinder tower at a high wind speed. *J. Wind Engng Ind. Aerodyn.* **69–71**, 731–744.

KONSTANTINIDIS, E. 2014 On the response and wake modes of a cylinder undergoing streamwise vortex-induced vibrations. *J. Fluids Struct.* **45**, 256–262.

KONSTANTINIDIS, E. & BALABANI, S. 2007 Symmetric vortex shedding in a near wake of a circular cylinder due to streamwise perturbations. *J. Fluids Struct.* **23**, 1047–1063.

KONSTANTINIDIS, E., BALABANI, S. & YIANNESKIS, M. 2003 The effect of flow perturbations on the near wake characteristics of a circular cylinder. *J. Fluids Struct.* **18**, 367–386.

KONSTANTINIDIS, E., BALABANI, S. & YIANNESKIS, M. 2007 Bimodal vortex shedding in a perturbed cylinder wake. *Phys. Fluids* **19**, 011701.

LEONG, C. M. & WEI, T. 2008 Two-degree-of-freedom vortex-induced vibrations of a pivoted cylinder below critical mass ratio. *Proc. R. Soc. Lond.* A **464**, 2907–2927.

LEVY, B. & LIU, Y. 2013 The effects of cactus inspired spines on the aerodynamics of a cylinder. *J. Fluids Struct.* **39**, 335–346.

MORSE, T. L. & WILLIAMSON, C. H. K. 2009 Prediction of vortex-induced vibration response by employing controlled motion. *J. Fluid Mech.* **634**, 5–39.

MORSE, T. L. & WILLIAMSON, C. H. K. 2010 Steady, unsteady and transient vortex-induced vibration predicted using controlled motion data. *J. Fluid Mech.* **649**, 429–451.

NAKAMURA, A., OKAJIMA, A. & KOSUGI, T. 2001 Experiments on flow-induced in-line oscillation of a circular cylinder in a water tunnel. *JSME Intl J.* **44** (4), 705–711 (2nd report, influence of aspect ratio of a cantilevered circular cylinder).

NAUDASCHER, E. 1987 Flow-induced streamwise vibrations of structures. *J. Fluids Struct.* **1**, 265–298.

NISHIHARA, T., KANEKO, S. & WATANABE, T. 2005 Characteristics of fluid dynamic forces acting on a circular cylinder oscillating in a streamwise direction and its wake patterns. *J. Fluids Struct.* **20**, 505–518.

OKAJIMA, A., KOSUGI, T. & NAKAMURA, A. 2001 Experiments on flow-induced in-line oscillation of a circular cylinder in a water tunnel. *JSME Intl J.* **4** (4), 695–704 (1st report, the difference of the response characteristics when a cylinder is elastically supported at both ends and cantilevered).

OKAJIMA, A., KOSUGI, T. & NAKAMURA, A. 2002 Flow-induced in-line oscillation of a circular cylinder in a water tunnel. *J. Press. Vessel Technol.* **124**, 89–96.

OKAJIMA, A., NAKAMURA, A., KOSUGI, T., UCHIDA, H. & TAMAKI, R. 2003 Flow-induced in-line oscillation of a circular cylinder. *Eur. J. Mech. (*B*/Fluids)* **23**, 115–125.

ONGOREN, A. & ROCKWELL, D. 1988 Flow structure from an oscillating cylinder Part 2. Mode competition in the near wake. *J. Fluid Mech.* **191**, 225–245.

PERDIKARIS, P. G., KAIKTSIS, L. & TRIANTAFYLLOU, G. S. 2009 Chaos in a cylinder wake due to forcing at the Strouhal frequency. *Phys. Fluids* **21**, 101705.

SANCHIS, A., SAELEVIK, G. & GRUE, J. 2008 Two-degree-of-freedom vortex-induced vibrations of a spring-mounted rigid cyliinder with low mass ratio. *J. Fluids Struct.* **24**, 907–919.

SARPKAYA, T. 1995 Hydrodynamic damping, flow-induced oscillations and biharmonic response. *Trans. ASME* **117**, 232–238.

SARPKAYA, T. 2004 A critical review of the intrinisic nature of vortex-induced vibrations. *J. Fluids Struct.* **19**, 389–447.

STANISLAS, M., OKAMOTO, K. & KÄHLER, C. 2003 Main results of the First International PIV Challenge. *Meas. Sci. Technol.* **14**, 63–89.

TECHET, A. H., HOVER, F. S. & TRIANTAFYLLOU, M. S. 1998 Vortical patterns behind a tapered cylinder oscillating transversely to a uniform flow. *J. Fluid Mech.* **363**, 79–96.

VAN OUDHEUSDEN, B. W., SCARANO, F., HINSBERG, N. P. & WATT, D. W. 2005 Phase-resolved characterization of vortex shedding in the near wake of a square-section cylinder at incidence. *Exp. Fluids* **39**, 86–98.

VOORHEES, A., ATSAVAPRANEE, P., BENAROYA, H. & WEI, T. 2008 Beating of a circular cylinder mounted as an inverted pendulum. *J. Fluid Mech.* **610**, 217–247.

VOORHEES, A. & WEI, T. 2002 Three-dimensionality in the wake of a surface piercing cylinder mounted as an inverted pendulum. In *Proceedings of BBVIV-3 Conference on Bluff Body Wakes and Vortex-Induced Vibrations, Port Douglas, Australia* (ed. K. Hourigan, K. Leweke, T. Thompson & C. H. K. Williamson) Monash University.

WILLIAMSON, C. H. K. & GOVARDHAN, R. 2004 Vortex-induced vibrations. *Annu. Rev. Fluid Mech.* **36**, 413–455.

WILLIAMSON, C. H. K. & JAUVTIS, N. 2004 A high-amplitude 2T mode of vortex-induced vibration for a light body in *XY* motion. *Eur. J. Mech. (*B*/Fluids)* **23**, 107–114.

WILLIAMSON, C. H. K. & ROSHKO, A. 1988 Vortex formation in the wake of an oscillating cylinder. *J. Fluids Struct.* **2**, 355–381.